sciendo Slovak Journal of Civil Engineering

Vol. 31, 2023, No. 2, 25 – 36
**DOI:** 10.2478/sjce-2023-0010

# EVALUATION OF A MEASUREMENT TURBULENCE MODEL OF THE WIND PRESSURE ON THE RUIN OF A FORTIFIED TOWER

Martin POLIAK[1*], Michal FRANEK[2], Jana GREGOROVÁ[1]

***Abstract***

*An analysis of the external pressure coefficient on the surface of a ruin in different flow directions is presented. The ruin has almost cube-like proportions with an open roof plane and a destroyed corner. Flow simulations were performed using 3D Time Steady RANS and compared with experimental results from the boundary layer wind tunnel at the Slovak University of Technology in Bratislava. The optimal turbulence model and internal mesh settings were selected based on their statistical evaluation. For an evaluation of the critical directions of the wind flow around the ruin, the values of the external wind pressure coefficient were obtained from the selected calculation model and settings.*

***Address***

[1] Dept. of Architecture, Faculty of Civil Engineering, Slovak University of Technology in Bratislava, Slovak Republic

[2] Dept. of Building Construction, Faculty of Civil Engineering, Slovak University of Technology in Bratislava, Slovak Republic

* ***Corresponding author:*** martin.poliak@stuba.sk

***Key words***

- Ruin protection,
- Wind tunnel,
- Computational fluid dynamics.

## 1 INTRODUCTION

In the context of monument protection, wind flow is of primary interest because of its destructive potential. As a destructive mechanism, it stresses the monument (a) mechanically and (b) chemically. Monuments are mechanically stressed by (aa) changing their surface integrity – for example, by grinding the surfaces of structures and removing elements of building materials loosened by freezing (e.g., plaster, mortar, or sedimentary rock layers in stone masonry); and by (ab) creating critical loads on structures, such as during extreme gales or storms, where not only elements prone to tearing off, such as roof coverings, but also stand-alone structures with compromised stability, are at risk. The wind contributes to the chemical stress on a monument (ba) by altering the water and gas chemical reactions caused by changes in pressure on it, or (bb) by transporting water, salts, sediments, and gaseous impurities (Sesana et al., 2021; Sabbioni et al., 2012; How, 2007).

The movement of the wind around a structure is greatly influenced by (a) the characteristics of the surrounding environment and (b) the characteristics of the structure itself. The characteristics of an environment can be described (aa) on a landscape scale by its orography, elevation, and orientation in the direction of any flow (Oláh et al., 2013; Global Wind Atlas); (ab) on an urban scale by the type of environment causing frictional forces on its surface, as expressed by the extent of its roughness, the type and density of the urban environment in which the structure is located, and by other interfering objects, such as neighboring greenery; and (ac) by the orientation of the structure against the flow (Liu et al., 2018; STN EN 1991-1-4, 2006). On an architectural scale, the flow is influenced by the characteristics of the structure (ba) its proportion, which is given by the ratio of the height of the structure to its width or depth (Mou et al., 2017), (bb) its shape, which is given by the geometry of the ground plan base of the structure, the type of roofing and its height from the base (Singh and Roy, 2019; Fouad et al., 2018), (bc) the spectrum of the architectural and constructional details of any peripheral structures, and (bd) the spectrum of building materials of any peripheral structures, which could affect the flow in the immediate vicinity of the surfaces of the structure.

© 2023 The Author(s). This is an open access article licensed under the Creative Commons Attribution 4 .0 License (https://creativecommons.org/licenses/by/4.0/)

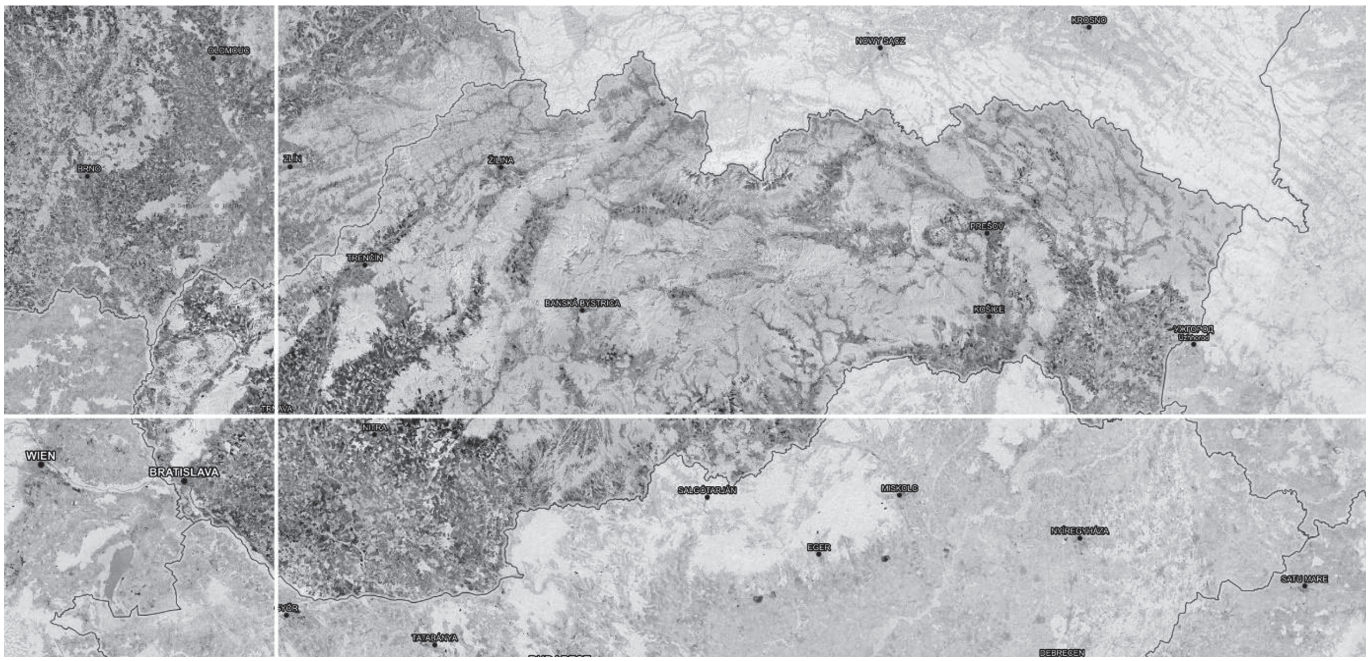



**Fig. 1** *Map of Slovakia; the cross is marking the location of the town of Trnava (©mapy.cz)*

With Computational Fluid Dynamics (CFD), the behaviour of the wind can be predicted from either the perspective of its own destructive mechanisms or from the perspective of another mechanism distributed by it. The use of CFD is used (a) to simulate wind movement in a given environment, (b) to analyse historical wind flow in an environment to confirm hypotheses related to interpretation, and (c) to make conservation design decisions (Grau-Bové et al., 2019). The simulation of wind movement in a certain environment was applied in the search for the most exposed and weathered places of the Giza plateau and the Great Sphinx by calculating the distribution of the friction and pressure coefficients and supplementing them with wind speed calculations (Hussein and El-Shishiny, 2009). As an aid to decision-making, wind flow simulations were used to estimate the wind-driven sand erosion of the Cardo stone colonnade of the Hispano-Romanesque site of Baelo Caludia in Cadíz, Spain (Pineda and Iranzo, 2017).

(Grau-Bové et al., 2019) examined the unusual employment of CFD in the cultural heritage context for the purposes of developing this computational methodology. That use is more focused on case studies and assistance in solving practical problems. The study also mentions how rare it is for simulations to be validated by another research method, which would serve to verify and calibrate the computational model and possibly bring the computational methodology closer to real-world results. This is primarily due to the long-term nature of simulations or because the problem to be solved is limited to simulating very slow interior flows, which are difficult to replicate experimentally. More than the wind itself, other destructive mechanisms such as the temperature, humidity, dust particles, or gaseous impurities distributed by the wind are of greater interest.

Philosophically, the present paper considers monuments as physical foundations of culturally and ecologically sustainable development and as the preservation of the genius loci, as reflected on different spatial scales and origins (Vecco, 2020; Pilař, 2016; Antrop, 2006; D'Acci, 2019; Nádaská and Pilař, 2017; Ruhig, 2017; Bránický and Gregorová, 2022). In so doing, the paper uses an idealised model of the ruin of the south-eastern corner tower of the Trnava fortifications, which has previously been identified as a significant location of cultural value and is currently undergoing actualisation of the monumental presentation (Gregorová, 2022). The tower has also been identified as one of the locations potentially vulnerable to climate change (Poliak, 2021). The external pressure coefficient $c_{pe}$ on the surface of the Trnava monument illustrates the flow and its impact on its substance. The calculations took place in the ANSYS Fluent software environment using alternatives that consider different flow directions, apply several types of turbulence models of the Reynolds-Averaged Navier-Stokes (RANS) turbulence, and change the internal settings of the domain and mesh of the calculations. A comparison is made between the calculations made at specific positions and the measurements taken in the Boundary Layer Wind Tunnel (BLWT) at the Slovak University of Technology in Bratislava (STU BA), to ensure the correct methodology in further research on the effectiveness of a roof in covering a ruin through its material protection. An optimal calculation model and alternative internal settings were selected using three statistical methods. Using the optimal calculation model, the most unfavourable flow directions around the ruin model were determined.

## 2 MATERIALS AND METHODS

### 2.1 Idealisation of the model of the selected ruin

The southeast corner tower of the fortification of the town of Trnava (Fig. 1), which is located between the grounds of the West Slovak Museum and the town amphitheatre (Fig. 2), is the subject of our research. Before losing its defensive functions and before its gradual destruction, it was a five-story building with an almost square base measuring approximate-




**Fig. 2** *Orthophoto of the town Trnava; the cross is marking the location of the southeast corner tower of the fortification (©mapy.cz)*

ly 8 × 8 m and with walls approximately 2.6 m thick on the lowest floor. The first four floors date back to the Romanesque period, while the fifth floor was added during the Baroque period by filling in battlements and adding a pyramidal roof. Each tower was connected by walls and had approximately three floors, including a parapet (Gregorová et al., 1996). At present, it is preserved at a height of two full floors with the impression of a third floor, an inner corner destroyed almost to ground level, and serrated front sides (typical of the presentation of a monumental fortification). Only the eastern curtain up to the height of the upper corridor has been preserved. The tower and the curtain are both the same height, with their masonry crowns capped with a concrete plate with a slight overlap (Fig. 3).

A portion of the urban context and architectural detail needed to be abstracted from the actual situation for the purpose of this work - (a) the configuration of the surrounding terrain, which is replaced by a plane with an averaged level height; (b) the surrounding buildings and greenery, creating interferences in the run-up area of the flow; (c) sections of walls (curtains) connected directly to the structure of the ruin; (d) architectural details such as overlaps of the concrete slab on the crowns of the masonry, serration of the wall faces, and the openings of slotted embrasures; and (e) the differences in the construction materials of the masonry and the slab, which is protecting the head of the masonry (Fig. 3).

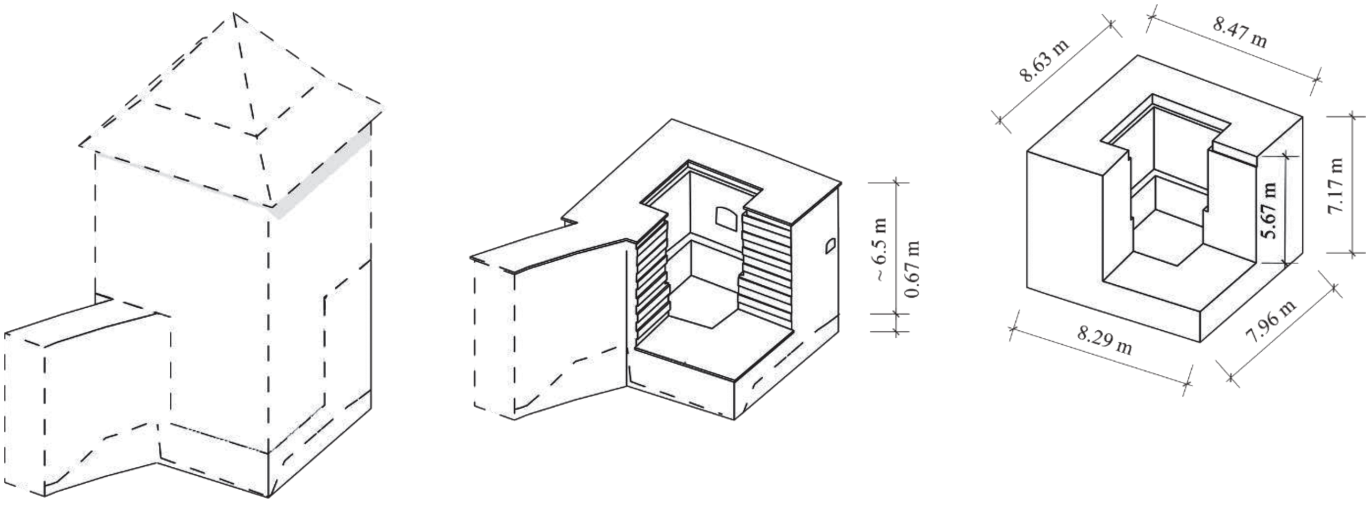



**Fig. 3** *Trnava's fortified tower of interest in its original, current, and idealised state*

### 2.2 Experimental measurement in BLWT STU BA

The Boundary Layer Wind Tunnel (BLWT), a low-speed tunnel with a length of 26.2 m and clear dimensions of 2.6 × 1.6 m (Hubová and Lobotka, 2014), was used for the experimental measurement of the external pressure coefficient $c_{pe}$ on the surface of the idealised ruin model. Based on the mean speed of the wind flow and the intensity of the turbulence, the roughness length $z_0$ = 0.7 m corresponds to the flow in a real-scale urbanized environment and the terrain categories III and IV according to the Eurocode (STN EN 1991-1-4, 2006). The external pressure coefficient $c_{pe}$ was calculated according to relation (1) based on the difference between the local static pressure in tap $p$ and the free stream mean static pressure $p_s$, air density $\rho$ = 1.164 kg·m$^{-3}$, and the reference flow velocity wind $v_{ref}$ = 7.871 m·s$^{-1}$:

$$c_{pe} = \frac{p - p_s}{\frac{1}{2}\rho v_{ref}^2} \tag{1}$$

A 3D printer was used to print the physical model on a 1:390 scale in PLA with a 0.3 mm profile width, 0.3 mm layer height, and final wall thickness of 4 mm with 100% infill. The model was fitted with 40 pressure taps at three heights: at the crown of the ruin's masonry as the highest horizontal plane, at two-thirds of the model's height, and at its foot in the open corner (Fig. 4). The flow was simulated in 16 directions in 22.5° steps.

### 2.3 Numerical calculation in CFD

The calculations took place in the ANSYS Fluent software environment in alternatives. The flow situations were simulated as pressure-based, time steady, and without a production limiter and curvature correction. The maximum residual value of all the quantities was set at $10^{-5}$. The simulations were performed in double precision on a desktop computer with an Intel® Core™ i7-10700K @ 3.80 GHz processor and 32.0 GB DDR4 RAM.

The dimensions of the computational domain were based on the height $H$ of the idealised model of the ruin on a scale of 1:390, i.e., on a scale identical to the dimensions of the physical model used for experimental measurements in the BLWT (Fig. 5) (Franke etal., 2007). The resulting volume of the computational domain was 19,965 m$^3$.

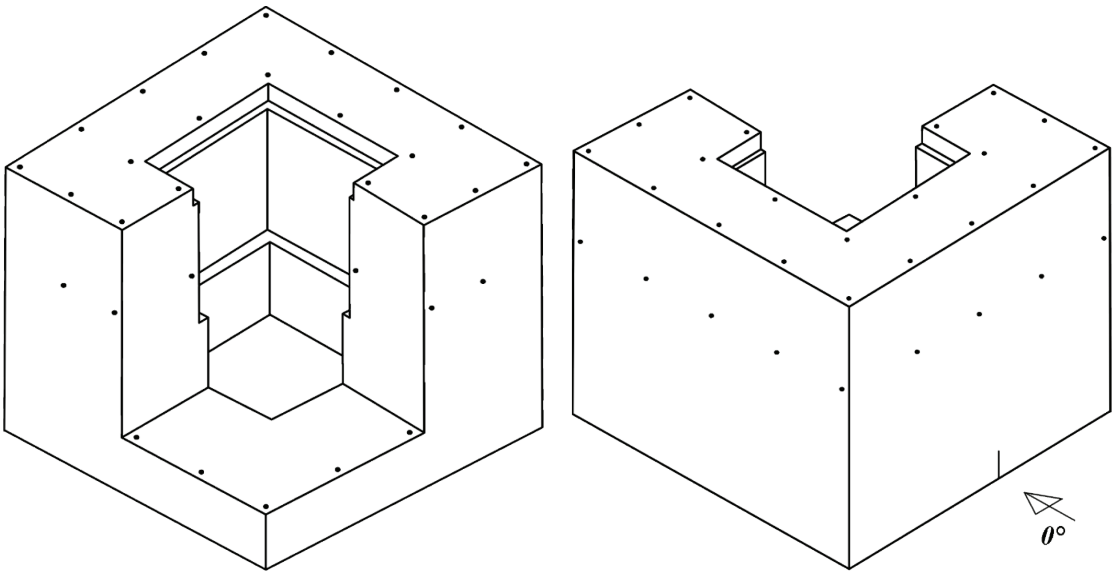



**Fig. 4** *Placement of pressure taps on the idealised physical model of the ruin*

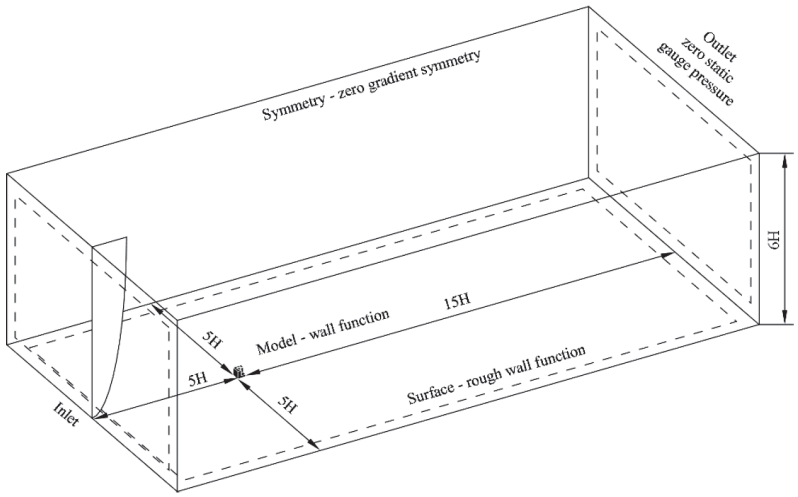



**Fig. 5** *Illustration of the computational domain's dimensions and boundary conditions*

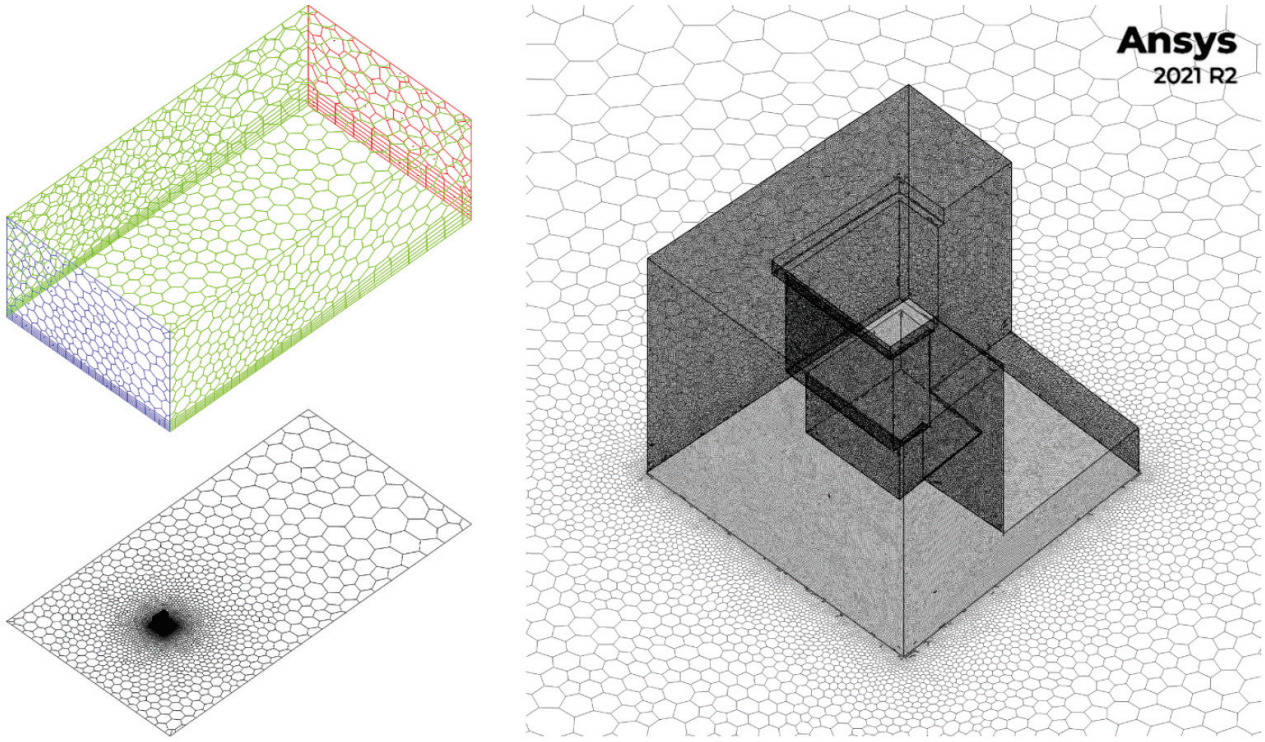



**Fig. 6** *Illustration of polyhedral mesh used; on the left, a blue inlet area, green symmetry area with a zero gradient, red outlet area, and a region of the terrain with a uniform roughness and with thickening mesh at the location of the idealised ruin model; on the right, details of the mesh on the surface of the idealised ruin model*

The computational mesh was modelled in the meshing component of the ANSYS Workbench environment. The growth rate for the sizing and inflation values was changed from the basic value of 1.2 to 1.1 for the model. In this case, the mesh was automatically created using tetrahedrons. An element face-sizing condition with a value of 1 mm and an inflation condition for the first five mesh layers with a height limitation of 1 mm for the first layer were entered for the surface of the ruin model. For the first five mesh layers, a smooth transition condition was also applied to the inflation condition on the terrain surface. There were approximately 7.5 million cells and 1.8 million nodes in the resulting tetrahedral mesh. The quality indicators included the mean orthogonal quality of 0.77 and mean skewness of 0.23 (Mesh Quality, 2022; Fatchurrohman and Chia, 2017; 6.2.2 Mesh Quality, 2009). From there, the mesh was directly converted to a polyhedral in Fluent (Fig. 6).

A logarithmic profile of the mean wind speed $v_m(z)$ was set at the input area of the computational domain according to the experimental measurements in BLWT:

$$v_m(z) = \frac{\dot{v}}{\kappa} ln \frac{z + z_0}{z_0} \tag{2}$$

where $v_m(z)$ is the mean wind speed at height $z$ above the terrain [m·s$^{-1}$]; $\dot{v}$ is the shear or friction velocity [m·s$^{-1}$]; $\kappa$ is the Von Kármán constant ($\kappa \approx 0.41$); $z$ is the height above the terrain [m]; and $z_0$ is the length of the roughness with a value of 0.00179 m, which is also set as a terrain with a uniform length of roughness. The following equations were used to specify other parameters in the input and output domain boundaries:

$$k(z) = \frac{\dot{v}^2}{\sqrt{C_\mu}} \tag{3}$$

$$\varepsilon(z) = \frac{\dot{v}^3}{\kappa(z + z_0)} \tag{4}$$

$$\omega(z) = \frac{\varepsilon}{k} \tag{5}$$

where $k(z)$ is the turbulent kinetic energy [m$^2$·s$^{-2}$]; $C_\mu$ is the constant of the $k$-$\varepsilon$ model; $\varepsilon$ is the dissipation rate of the turbulent kinetic energy [m$^2$·s$^{-3}$]; and $\omega(z)$ is the specific dissipation of the turbulent kinetic energy [s$^{-1}$]. The sides and top of the computational domain were set as symmetrical boundaries with a zero gradient. The surface of the idealised ruin model had a roughness height set at 0.5 mm with a roughness constant of 0.5, while the terrain had a roughness height of 1.79 mm with a constant of 0.7.

A series of Reynolds-Averaged Navier-Stokes (RANS) turbulence models were used to simulate the eight wind directions in 45° steps, namely, Standard $k$–$\varepsilon$ (sKE), Realizable $k$–$\varepsilon$ (rKE), Re-Normalization Group $k$–$\varepsilon$ (rngKE), Standard $k$–$\omega$ (sKO), Generalised $k$–$\omega$ (gekoKO), New Baseline $k$–$\omega$ (bslKO), and Shear Stress Transport $k$–$\omega$ (sstKO) (Menter et al., 2021; Menter, 1994; CFD Online, n.d.).

In order to further verify the computational model, several variants of the internal settings of the computational domain and mesh for one flow direction were applied, as shown in Tab. 1 and Fig. 7.

**Tab. 1** *Summary of the internal domain and mesh settings*

| | Mesh | | | | | | | | | *k-ε* Wall Treatment |
|---|---|---|---|---|---|---|---|---|---|---|
| | Sizing | | Inflation 5 layers | | | Elements [mil] | Nodes [mil] | Quality | | |
| | Growth Rate | Ruin Model | Growth Rate | Ruin Model | Surface | | | Ortho. | Skew. | |
| **1** | *1.1* | *Face 1 mm* | *1.1* | *FLT 1 mm* | *Smooth Trans.* | *7.5* | *1.8* | *0.77* | *0.23* | *Stand.* |
| **2** | *1.1* | *Face 1 mm* | *1.1* | *x* | *x* | *9.2* | *1.6* | *0.78* | *0.22* | *Stand.* |
| **3** | *1.1* | *x* | *1.2* | *FLT 1.1 mm* | *FLT 3.6 mm* | *0.5* | *0.3* | *0.76* | *0.24* | *Stand.* |
| **4** | *1.1* | *x* | *1.2* | *FLT 1.1 mm* | *FLT 3.6 mm* | *0.5* | *0.3* | *0.76* | *0.24* | *Enhan.* |
| **5** | *1.1* | *Edge 1 mm* | *1.2* | *FLT 1.1 mm* | *FLT 3.6 mm* | *4.2* | *2.5* | *0.75* | *0.25* | *Enhan.* |
| **6** | *1.1* | *Edge 2 mm* | *1.2* | *FLT 1.1 mm* | *FLT 3.6 mm* | *1.9* | *1.1* | *0.75* | *0.25* | *Enhan.* |

**Tab. 2** *Statistical evaluation of the results calculated in CFD by various turbulence models, which considered eight flow directions; the most positive values are in black, the most negative in gray; note that all the FB values are negative, meaning that the CFD results are overestimated in comparison to the BLWT results.*

| | | sKE | rngKE | rKE | sKW | gekoKW | bslKW | *sstKW* | I.V. |
|---|---|---|---|---|---|---|---|---|---|
| **0°** | *FB* | *-0.245* | *-0.223* | *-0.260* | *-0.288* | *-0.248* | *-0.284* | *-0.183* | **0** |
| | *R* | *0.820* | *0.916* | *0.838* | *0.851* | *0.864* | *0.845* | *0.950* | **1** |
| | *FAC1.3* | *0.300* | *0.625* | *0.375* | *0.375* | *0.400* | *0.425* | *0.875* | **1** |
| **45°** | *FB* | *-0.169* | *-0.178* | *-0.169* | *-0.229* | *-0.187* | *-0.208* | *-0.113* | **0** |
| | *R* | *0.896* | *0.912* | *0.896* | *0.878* | *0.898* | *0.874* | *0.915* | **1** |
| | *FAC1.3* | *0.700* | *0.650* | *0.625* | *0.575* | *0.675* | *0.600* | *0.675* | **1** |
| **90°** | *FB* | *-0.152* | *-0.195* | *-0.180* | *-0.226* | *-0.200* | *-0.216* | *-0.153* | **0** |
| | *R* | *0.914* | *0.936* | *0.919* | *0.917* | *0.927* | *0.912* | *0.949* | **1** |
| | *FAC1.3* | *0.525* | *0.575* | *0.525* | *0.450* | *0.475* | *0.500* | *0.700* | **1** |
| **135°** | *FB* | *-0.106* | *-0.167* | *-0.172* | *-0.187* | *-0.172* | *-0.179* | *-0.126* | **0** |
| | *R* | *0.898* | *0.939* | *0.933* | *0.880* | *0.927* | *0.874* | *0.941* | **1** |
| | *FAC1.3* | *0.775* | *0.725* | *0.700* | *0.600* | *0.700* | *0.700* | *0.700* | **1** |
| **180°** | *FB* | *-0.148* | *-0.194* | *-0.182* | *-0.224* | *-0.200* | *-0.216* | *-0.151* | **0** |
| | *R* | *0.872* | *0.931* | *0.891* | *0.888* | *0.898* | *0.862* | *0.931* | **1** |
| | *FAC1.3* | *0.575* | *0.550* | *0.500* | *0.475* | *0.550* | *0.475* | *0.675* | **1** |
| **225°** | *FB* | *-0.108* | *-0.143* | *-0.127* | *-0.205* | *-0.151* | *-0.174* | *-0.084* | **0** |
| | *R* | *0.911* | *0.940* | *0.913* | *0.878* | *0.911* | *0.875* | *0.930* | **1** |
| | *FAC1.3* | *0.725* | *0.675* | *0.750* | *0.575* | *0.750* | *0.575* | *0.800* | **1** |
| **270°** | *FB* | *-0.208* | *-0.216* | *-0.237* | *-0.270* | *-0.226* | *-0.254* | *-0.176* | **0** |
| | *R* | *0.804* | *0.897* | *0.816* | *0.849* | *0.841* | *0.844* | *0.923* | **1** |
| | *FAC1.3* | *0.375* | *0.525* | *0.300* | *0.325* | *0.375* | *0.325* | *0.725* | **1** |
| **315°** | *FB* | *-0.191* | *-0.248* | *-0.255* | *-0.287* | *-0.243* | *-0.239* | *-0.195* | **0** |
| | *R* | *0.894* | *0.926* | *0.903* | *0.863* | *0.898* | *0.862* | *0.919* | **1** |
| | *FAC1.3* | *0.800* | *0.675* | *0.625* | *0.475* | *0.650* | *0.625* | *0.725* | **1** |

### 2.4 Assessment of results and method of comparison

Three statistical methods were applied to assess the results: fractional bias (FB; ideal value (I.V.) = 0.0), correlation coefficient (R, I.V. = 1.0), and part of the results within factor 1.3 (FAC1.3, IV = 1.0) based on the following equations:

$$FB = 2\frac{\bar{X} - \bar{Y}}{\bar{X} + \bar{Y}} \tag{6}$$

$$R = \frac{cov(X,Y)}{\sigma_X \sigma_Y} \tag{7}$$

$$FAC1.3 = \frac{1}{n}\sum_{i=1}^{n} N_i, where\ N_i = \begin{Bmatrix} 1\ for\ \frac{1}{1.3} \le \frac{X_i}{Y_i} \le 1.3 \\ 0\ for\ others \end{Bmatrix} \tag{8}$$

where $\bar{X}$ is the average of the $c_{pe}$ values measured in BLWT; $X$ is the $c_{pe}$ value measured in BLWT; $\bar{Y}$ is the average $c_{pe}$ value calculated in CFD; $Y$ is the $c_{pe}$ value calculated in CFD; $cov$ is the covariance; and $\sigma_X$, $\sigma_Y$ are the standard deviations for $X$ and $Y$ (Franek et al., 2021).

## 3 RESULTS

The experimental results from BLWT were compared with the CFD results calculated using seven turbulence models, which considered eight directions of flow from 0° to 315° in 45° steps (Tab. 2).

The results from the experimental measurements in BLWT were subsequently compared with those calculated in CFD using variant internal computational domain and mesh settings and analysed using the same statistical methods (Tab. 3).

Once the previous two steps were evaluated and the optimal turbulence model (sstKW), calculation domain, and mesh internal settings were selected (combination #1), the next step was to analyse the most critical flow directions. As a result of the $c_{pe}$ values calculated for the entire surface of the idealised ruin model, the extreme values were assessed: the greatest and lowest values $c_{pe,max}$ and $c_{pe,min}$, which were followed by the average and median $c_{pe,mean}$ and $c_{pe,M}$ values (Tab. 4). The flow directions, which deviated by 22.5° on both sides, were supplemented near the critical directions estimated in the first round of the analysis (Tab. 5).

## 4 DISCUSSION

As shown in Tabs. 2 and 3, negative values were observed throughout the comparison of the BLWT and CFD data by using the FB statistical method, which indicates that the CFD results were overestimated.

Tab. 2 marks the most accurate sstKW turbulence model. However, for some flow directions, the positive results from the data comparison point to the sKE and rngKE calculation models. Compared to the others, the sstKW model did not pro-

**Tab. 3** *Statistical analysis of the results calculated in CFD by different computational models of turbulence, which considered six different combinations of the computational domain and mesh; note that all the FB values are negative, meaning that the CFD results are overestimated in comparison to the BLWT results.*

| | | sKE | rngKE | rKE | sKW | gekoKW | bslKW | sstKW | I.V. |
|---|---|---|---|---|---|---|---|---|---|
| 1 | FB | -0.197 | -0.159 | -0.199 | -0.257 | -0.199 | -0.256 | -0.145 | 0 |
| | R | 0.829 | 0.930 | 0.857 | 0.856 | 0.875 | 0.848 | 0.951 | 1 |
| | FAC1.3 | 0.313 | 0.781 | 0.469 | 0.438 | 0.469 | 0.406 | 0.875 | 1 |
| 2 | FB | -0.196 | -0.261 | -0.231 | -0.261 | -0.236 | -0.261 | -0.224 | 0 |
| | R | 0.877 | 0.933 | 0.913 | 0.853 | 0.914 | 0.831 | 0.951 | 1 |
| | FAC1.3 | 0.500 | 0.344 | 0.469 | 0.406 | 0.500 | 0.219 | 0.656 | 1 |
| 3 | FB | -0.186 | -0.236 | -0.206 | -0.255 | -0.193 | -0.256 | -0.200 | 0 |
| | R | 0.795 | 0.895 | 0.825 | 0.832 | 0.823 | 0.829 | 0.939 | 1 |
| | FAC1.3 | 0.219 | 0.375 | 0.250 | 0.063 | 0.188 | 0.094 | 0.625 | 1 |
| 4 | FB | -0.187 | -0.236 | -0.207 | | | | | 0 |
| | R | 0.794 | 0.895 | 0.825 | | | | | 1 |
| | FAC1.3 | 0.219 | 0.375 | 0.250 | | | | | 1 |
| 5 | FB | -0.236 | -0.254 | -0.244 | -0.224 | -0.239 | -0.227 | -0.247 | 0 |
| | R | 0.842 | 0.938 | 0.849 | 0.856 | 0.880 | 0.846 | 0.947 | 1 |
| | FAC1.3 | 0.219 | 0.438 | 0.250 | 0.156 | 0.250 | 0.125 | 0.344 | 1 |
| 6 | FB | -0.218 | -0.251 | -0.233 | -0.221 | -0.235 | -0.225 | -0.219 | 0 |
| | R | 0.824 | 0.936 | 0.830 | 0.859 | 0.897 | 0.848 | 0.950 | 1 |
| | FAC1.3 | 0.250 | 0.469 | 0.250 | 0.156 | 0.438 | 0.125 | 0.625 | 1 |

duce any negative results. From this point of view, the data from the sKW, sKE and rKE models appear to be the least accurate.

Tab. 3 represents the most accurate sstKW turbulence model in the first combination of the computational domain and internal mesh settings. Later combinations yielded more positive results only within their specific calculation models.

Tab. 4 denotes the three flow directions as critical: (1) 0° in terms of the average value and the median value of the external pressure coefficients $c_{pe,mean}$ and $c_{pe,M}$; (2) 225° in terms of the highest value captured of the maximum external pressure coefficient $c_{pe,max}$, the lowest value of the minimum external pressure coefficient $c_{pe,min}$, and also one of the highest values $c_{pe,mean}$ captured; and similarly, (3) the 315° direction captured the most

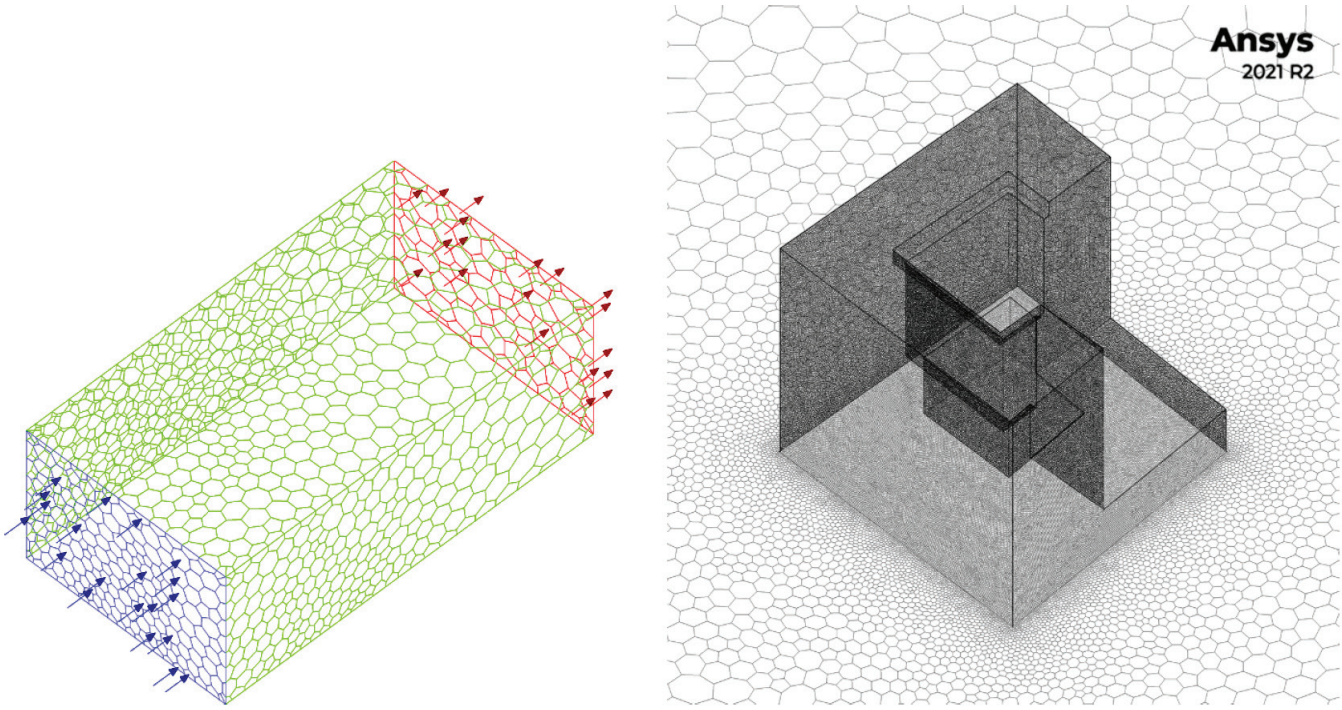



**Fig. 7** *Illustration of differences in the computation meshes considering the different variants of the settings; on the left, a view of the entire computational domain; on the right, a detail of the surface of the idealised ruin model; variant 2 from Tab. 3.*

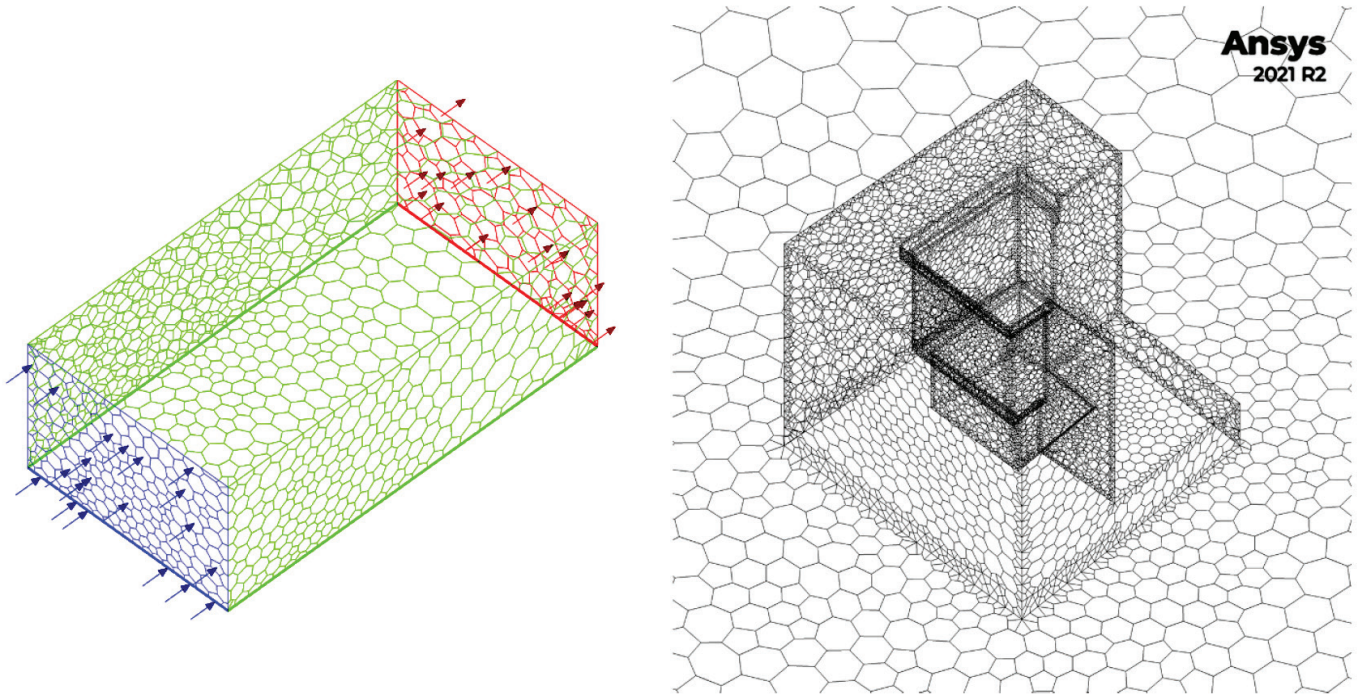



**Fig. 8** *Illustration of differences in the computation meshes considering the different variants of the settings; on the left, a view of the entire computational domain; on the right, a detail of the surface of the idealised ruin model; variants 3-4 from Tab. 3.*

extreme values of $c_{pe,max}$, $c_{pe,min}$ and $c_{pe,M}$. However, some parameters monitored were directed at secondary flow directions. Therefore, the second analysis of the critical flow directions was supplemented with additional flow directions deviating by 22.5° on both sides of the three critical directions assessed previously.

The second analysis is summarized in Tab. 5. The 22.5° direction was evaluated as the most critical flow direction, because it was the only one that captured three extreme values of the four parameters monitored; and 247.5° because of the high values of the mean and median of the external pressure coefficients $c_{pe,mean}$ and $c_{pe,M}$. The second analysis confirmed the 315° flow direction as critical (Fig. 11).

In each of the cirtical flow directions $c_{pe,max}$ was monitored at the windward face of the model and the $c_{pe,min}$ value at the

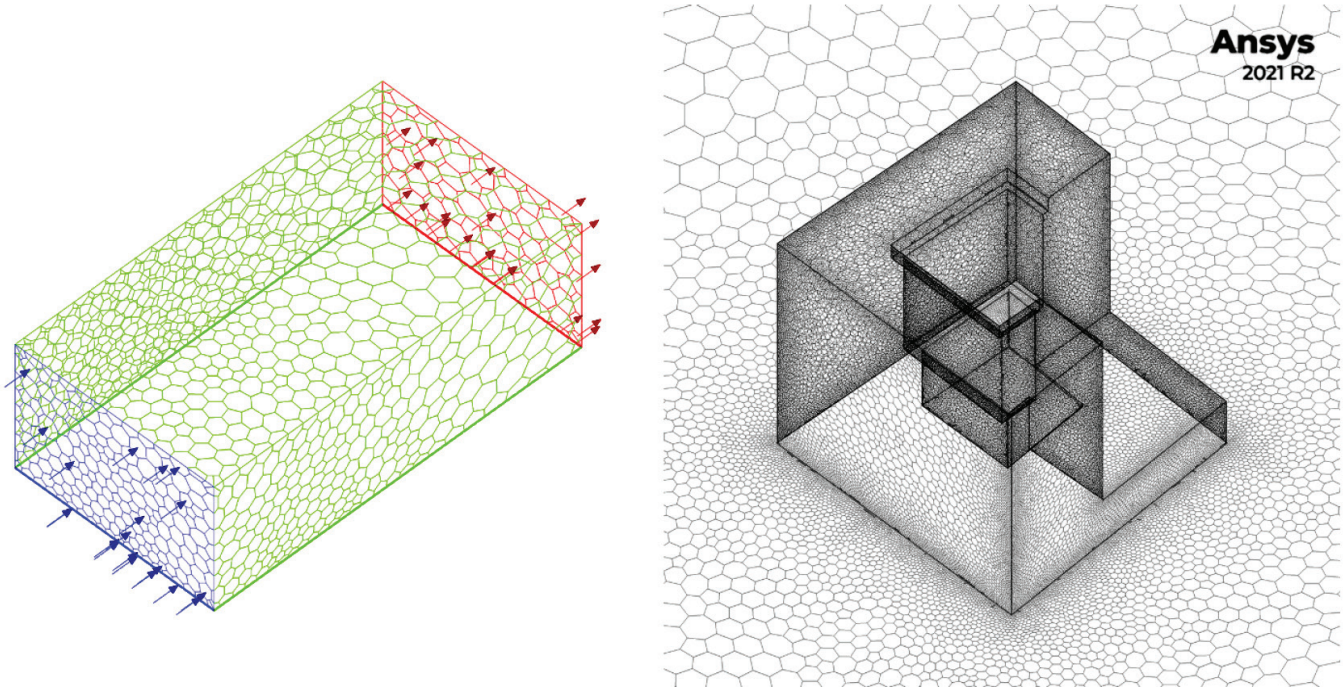



**Fig. 9** *Illustration of differences in the computation meshes considering the different variants of the settings; on the left, a view of the entire computational domain; on the right, a detail of the surface of the idealised ruin model; variant 5 from Tab. 3.*

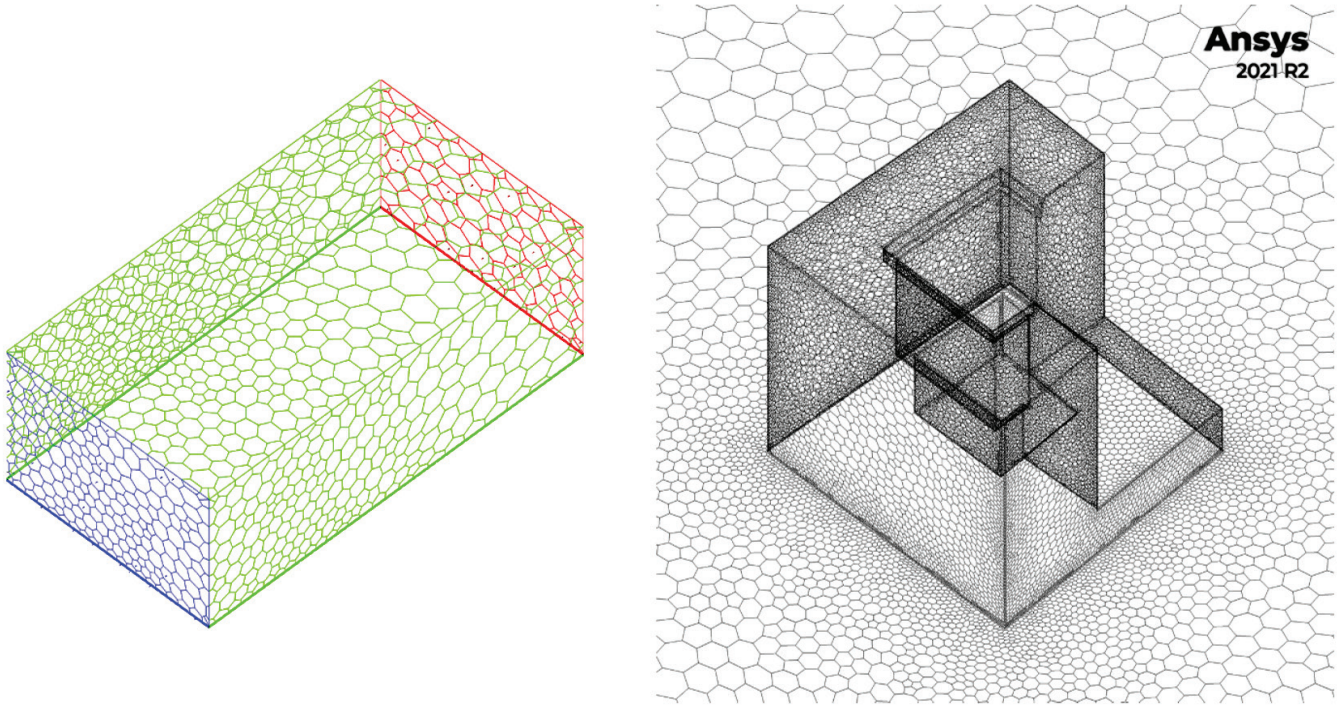



**Fig. 10** *Illustration of differences in the computation meshes considering the different variants of the settings; on the left, a view of the entire computational domain; on the right, a detail of the surface of the idealised ruin model; variant 6 from Tab. 3.*

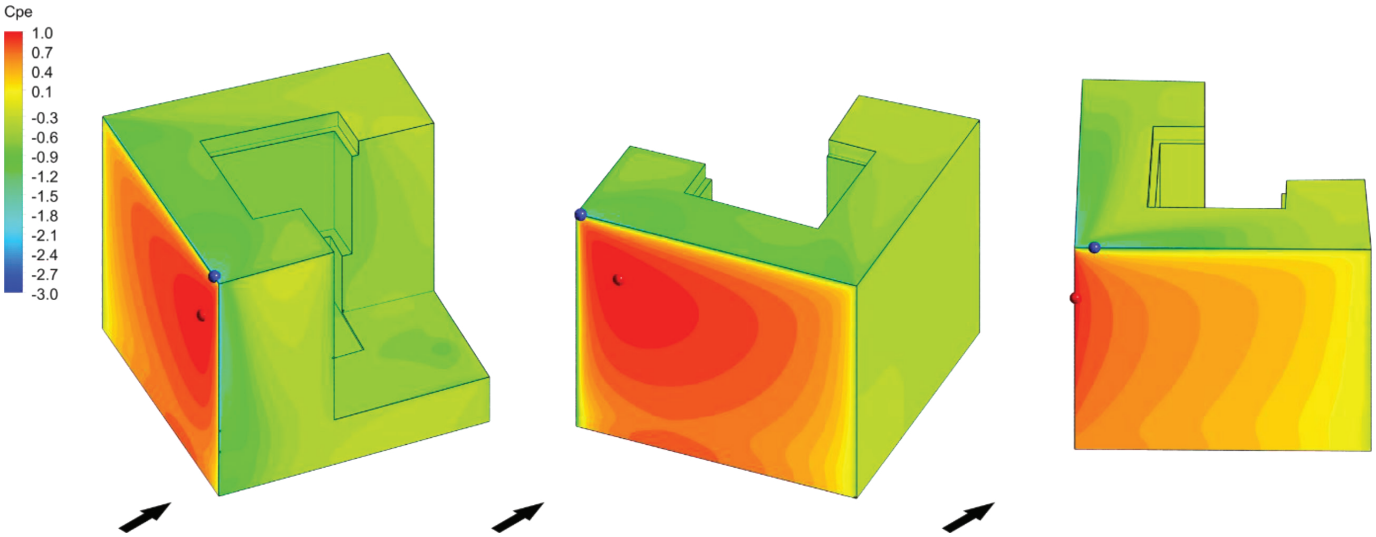



**Fig. 11** *Distribution of the external pressure coefficient $c_{pe}$ illustration for flow directions 22.5°, 247.5° and 315°, with locations of $c_{pe,max}$ (red) and $c_{pe,min}$ (blue).*

edge, where the windward face meets the head of the model's walls (Fig. 11).

## 4 CONCLUSION

Based on a statistical analysis of the values of the external pressure coefficient $c_{pe}$ at 40 taps on the surface of the idealised ruin model, the sstKW turbulence model has been evaluated as the most appropriate model. These values were obtained by both experimental measurements in BLWT and numerical calculations in CFD during the simulation of eight flow directions. An additional evaluation of the combination of the computational mesh and the domain internal settings for one flow direction was conducted to verify the suitability of the sstKW turbulence model, based on a statistical analysis of the results. The critical flow directions of 22.5°, 247.5° and 315° were analysed and evaluated, based on the maximum, minimum, mean, and median values of the external pressure coefficient $c_{pe}$ on the surface of the idealised ruin model, which was obtained by calculations in the optimized sstKW turbulence model.

*Acknowledgements*

As part of the Program for Support of Young Researchers at the Slovak University of Technology in Bratislava, the equipment for the construction of a idealised physical ruin model was purchased through the project *Simulation of the impact of the shape of the roof over the ruin on the distribution of wind pressure in critical areas* (BOREAS). A physical model of the ruin was created on the 3D printers at the Department of Architecture of the Faculty of Architecture of the Slovak University of Technology in Bratislava, which was acquired with the support of the *Penta Foundation*.

## REFERENCES


**6.2.2 Mesh Quality (2009)** *ANSYS FLUENT 12.0/12.1 Documentation* (online). (accessed 2023-03-03). Available at: www.afs.enea.it/project/neptunius/docs/fluent/html/ug/node167.htm

**Antrop, M. (2006)** *Sustainable landscapes: contradiction, fiction or utopia?* Landscape and Urban Planning (online), 75(3- 4), 187-197 (accessed 2023-05-09). DOI: 10.1016/j.landurbplan.2005.02.014. ISSN 01692046

**Bránický, F. - Gregorová, J. (2022)** *Searching for lost identity of Orava countryside.* In: Peřinková, M. - Jüttnerová, S. - Videcká, L. 14th Architecture in Perspective 2022. Ostra-va, CZ: VŠB - Technical University of Ostrava, pp. 84-89.

***CFD Online*** (online). n.d. (accessed 2021-07-22). Available at: http://www.cfd-online.com/

**D'Acci, L. (2019)** *A new type of cities for liveable futures.* Isobenefit Urbanism morphogenesis. Journal of Environmental Management (online), pp. 128-140 (accessed 2023-05-09). DOI: 10.1016/j.jenvman.2019.05.129. ISSN 03014797

**Fatchurrohman, N. - Chia, S. (2017)** *Performance of hybrid nano-micro reinforced mg metal matrix composites brake calliper: simulation approach.* IOP Conference Series: Materials Science and Engineering (online), 257 pp. (accessed 2023-03- 03). DOI: 10.1088/1757-899X/257/1/012060. ISSN 1757-8981

**Fouad, N. - Mahmoud, G. - Nasr N. (2018)** *Comparative Study of International Codes Wind Loads and CFD Results for Low-Rise Buildings.* Alexandria Engineering Journal (online), 57(4), 3623-3639 (accessed 2021-07-22). DOI: 10.1016/j. aej.2017.11.023. ISSN 11100168.

**Franek, M. - Macák, M. - Hubová, O. - Ivánková, O. (2021)** *Impact of Turbulence Models of Wind Pressure on Two Buildings with Atypical Cross-Sections*. Civil and Environmental Engineering (online), 17(2), 409-419 (accessed 2023-02-28). DOI: 10.2478/cee-2021-0044. ISSN 2199-6512

**Franke, J. - Hellsten, A. - H. Schlünzen - B. Carissimo, eds. (2007)** *Best Practice Guidelines for the CFD Simulation of Flows in the Urban Environment.* Hamburg, DE: COST Office. ISBN 3-00-018312-4.

**Global Wind Atlas** (online). n.d. (accessed 2021-06-29). Available at: http://globalwindatlas.info/

**Grau-Bové, J. - Mazzei, L. - Strlic, M. - Cassar, M. (2019)** *Fluid simulations in heritage science.* Heritage Science (online), 7(1) (accessed 2021-07-28). DOI: 10.1186/s40494-019- 0259-9. ISSN 2050-7445

**Gregorová, J. - Staník I. - Brtková, B. - Galajdová, J. (1996)** *Koncepcia prezentácie hradobného systému MPR Tr-nava (Concept of Presentation of the Fortification of the Town of Trnava).*

**Gregorová, J. (2022)** *Príprava komplexnej obnovy NKP mestského opevnenia v Trnave (Preparation of Complex Renovation of National Cultural Monument of the Fortification of the Town of Trnava): Pilotný projekt Katedry UNESCO pre obnovu architektonického dedičstva na STU v Bratislave (1. etapa) (Pilot Project of the UNESCO Chair for Preservation of the Architectural Heritage at Slovak University of Technology in Bratislava (1st phase)).* In: Archinfo (online). (accessed 2023-03-05). Available at: www.archinfo.sk/diskusia/blog/diela/priprava-komplexnej-obnovy-nkp-mestskeho-opevnenia-v-trnave-pilotny-projekt-katedry-unesco-pre-obnovu-architektonickeho-dedicstva-na-stu-v-bratislave-1-etapa.html

**How, C. (2007)** *Stability and survival*. In: ASHURST, J. *Conservation of Ruins*. 1. UK: Butterworth-Heinermann, pp. 11-43. ISBN 978-0-75-066429-5

**Hubová, O. - Lobotka, P. (2014)** *The Multipurpose New Wind Tunnel STU*. Civil and Environmental Engineering (online), 10(1), 1-9 (accessed 2023-02-28). DOI: 10.2478/cee-2014-0001. ISSN 1336-5835

**Hussein, A. - El-Shishiny, H. (2009)** *Wind Flow Modeling and Simulation over the Giza Plateau Cultural Heritage Site in Egypt*. Journal on Computing and Cultural Heritage (online), 2(2), 1-22 (accessed 2021-07-28). DOI: 10.1145/1613672.1613674. ISSN 1556-4673

**Liu, S. - Pan, W. - Zhao, X. - Zhang, H. - Cheng, X. - Long, Z. - Chen, Q. (2018)** *Influence of surrounding buildings on wind flow around a building predicted by CFD simulations.* Building and Environment (online), 140, 1-10 (accessed 2021-07-22). DOI: 10.1016/j.buildenv.2018.05.011. ISSN 03601323

**Menter, F. R. (1994)** *Two-equation eddy-viscosity turbulence models for engineering applications.* AIAA Journal (online), 32(8), 1598-1605 (accessed 2023-02-27). DOI: 10.2514/3.12149. ISSN 0001-1452

**Menter, F. - Lechner, R. - Matyushenko, A. (2021)** *Best Practice: RANS Turbulence Modeling in Ansys CFD* (online). 1.0. ANSYS, Inc. (accessed 2023-02-27). Available at: https://www.ansys.com/resource-center/technical-paper/best-practice-rans-turbulence-modeling-in-ansys-cfd

**Mesh Quality** (2022) *SimScale* (online). (accessed 2023-03-03). Available at: www.simscale.com/docs/simulation-setup/meshing/mesh-quality/

**Mou, B. - He, B. - Zhao, D. - Chau, K. (2017)** *Numerical simulation of the effects of building dimensional variation on wind pressure distribution*. In: Engineering Applications of Computational Fluid Mechanics (online), 11(1), 293-309 (accessed 2021-07-22). DOI: 10.1080/19942060.2017.1281845. ISSN 1994-2060

**Nádaská, Z. - Pilař, P. (2017)** *Conceptual Solution for the Revitali - zation of Public Spaces in Slovak Towns: Case Study: Stupava*. In: PEŘINKOVÁ, M. - NEDVĚD, M. 9th Architecture in Pespective 2017. Ostrava, CZ: VŠB - Technical University of Ostrava, pp. 177-180. ISBN 978-80-248-4058-1

**Oláh, J. - Rusnák, R. - Urbánek, M. Žiak, V. (2013)** *Konštrukcie pozemných stavieb III (Structures of Buildings III): Strechy budov (Roofs of Buildings).* SR: Slovak University of Technology in Bratislava. ISBN 978-80-227-3635-0

**Pilař, P. (2016)** *KULTURFABRIK: Harmony of Unconventional Art and Conversion of Buildings.* In: PEŘINKOVÁ, M. - NEDVĚD, M. 8th Architecture in Perspective 2016. Ostrava, CZ: VŠB - Technical University of Ostrava, pp. 231-233. ISBN 978-80-248-3940-0

**Pineda, P. - Iranzo, A. (2017)** *Analysis of sand-loaded air flow erosion in heritage sites by Computational Fluid Dynamics: Method and damage prediction*. Journal of Cultural Heritage (online), 25, 75-86 (accessed 2021-07-28). DOI: 10.1016/j.culher.2016.12.005. ISSN 12962074

**Poliak, M. (2021)** *Climatic Exposure of Slovak Ruins.* In: Advances in Architectural, Civil and Environmental Engineering. Bratislava, SK: Spektrum STU. ISBN 978-80-227-5150-6

**Ruhig R. (2017)** *Preservation of Historic Elements by Application Winter Gardens on the Facade of a Residential Building in Madrid*. In: PEŘINKOVÁ, M. - NEDVĚD, M. 9th Architecture in Pespective 2017. Ostrava, CZ: VŠB - Technical University of Ostrava, pp. 254-255. ISBN 978-80-248-4058-1

**Sabbioni, C. - Brimblecombe, P. - Cassar, M. (2012)** *The Atlas of Climate Change Impact on European Cultural Heritage: Scientific Analysis and Management Strategies*. UK: Anthem Press. DOI: 10.2777/11959. ISBN 978-92-79-25377-5

**Sesana, E. - Gagnon, A. - Ciantelli, C. - Cassar, J. - Hughes, J. (2021)** *Climate change impacts on cultural heri-tage: A literature review.* WIREs Climate Change (online), 12(4) (accessed 2021-07-22). DOI: 10.1002/wcc.710. ISSN 1757-7780

**Singh, J. - Roy, A. (2019)** *Effects of Roof Slope and Wind Direction on Wind Pressure Distribution on the Roof of a Square Plan Pyramidal Low-Rise Building Using CFD Simulation.* International Journal of Advanced Structural Engineering (online), 11(2), 231-254 (accessed 2021-07-22). DOI: 10.1007/s40091-019-0227-3. ISSN 2008-3556

**STN EN 1991-1-4. (2006)** *Eurokód 1: Zaťaženia konštrukcií (Eurocode 1: Actions on Structures): Časť 1-4: Všeobecné zaťaženia - Zaťaženie vetrom (Part I-IV: General Actions - Wind Actions).* Bratislava, SK: Slovak Office of Standards, Metrology and Testing.

**Vecco, M. (2020)** *Genius loci as a meta-concept*. Journal of Cultu - ral Heritage (online), 41, 225-231 (accessed 2023-05-09). DOI: 10.1016/j.culher.2019.07.001. ISSN 12962074